Engineering Journal issn: 0125-8281

Article

Buckling Analysis of Nonlocal Nanocolumns Using Finite Element Method

Tosporn Prasertsri[1,a,*], Suppawit Intratanoo[2,b], Thunyamas Jirajaran[2,c], Weeraporn Phongtinnaboot[3,d], and Jaroon Rungamornrat[2,e]

1 Department of Civil Engineering, Faculty of Engineering and Architecture, Rajamangala University of Technology Tawan-ok, Bangkok, Thailand
2 Department of Civil Engineering, Faculty of Engineering, Chulalongkorn University, Bangkok, Thailand
3 Department of Civil Engineering, Faculty of Engineering, Burapha University, Chonburi, Thailand
E-mail: [a,*]tosporn_pr@rmutto.ac.th (Corresponding author), [b]isuppawit@gmail.com, [c]thunyamas-ploy@hotmail.com, [d]weeraporn@buu.ac.th, [e]jaroon.r@chula.ac.th

Abstract. This research introduces a finite element method, considering size-dependent effect via nonlocal elasticity to analyze the buckling load of columns subjected to concentrated, distributed, and combined load cases. Two types of columns are considered: columns with a constant moment of inertia and nonuniform cross-section. The end conditions of columns comprise the following: clamped-free, hinged–hinged, clamped–hinged, and clamped–clamped. This paper illustrates the computational results using the relationship between buckling load normalized via the classical eigenvalue buckling load. The current findings show that the buckling load dramatically decreases at the normalized material length scale between 1 and 10. The most and least considerable effects on buckling load reduction are clamped–clamped and clamped-free end conditions. For the case of combined loads, a buckling concentrated load decreased proportionally as applied uniformly distributed force increased. An increase in concavity (or convexity) of parabolic columns will influence the buckling of the concentrated and uniformly distributed buckling loads.

Keywords: Column, elastic buckling, Eringen's integral model, nonlocal elasticity.

ENGINEERING JOURNAL Volume 26 Issue 10
Received 14 May 2022
Accepted 18 October 2022
Published 31 October 2022
Online at https://engj.org/
DOI:10.4186/ej.2022.26.10.73

DOI:10.4186/ej.2022.26.10.73

1. Introduction

Structural behavior considering the bending, buckling, and vibration of beam–column-like components of micro-electro-mechanical systems (MEMSs) and nano-electro-mechanical systems (NEMSs) has been widely investigated in previous works [1-3]. Such a wide investigation is due to the numerous real-world applications of these systems, such as 3D-printed micro-trusses, electrically-driven semiconductor lasers, optomechanical resonators, photonic crystals, transistors, and vibration shock sensors [4-9]. Many researchers have proposed various mathematical frameworks for modeling the structural behavior of micro/nano-beam–column members in minuscule structures to avoid time-consuming and uneconomical experiments. An analysis of structural members in MEMSs and NEMSs requires additional assumptions of continuum theories to capture the small-scale effect and long-distance interaction. Many approaches are also used to predict a type of mechanical behavior of atomic structures. Well-known examples of size-dependent continuum theories include modified couple stress elasticity theory [10-12], strain gradient theory [13, 14], stress-driven elasticity theory [15, 16], and doublet mechanics theory [17, 18]. A simple and longstanding theory, known as Eringen's nonlocal model, exists [19]. This theory has been recognized as an alternative to address the size-dependent response of any system through a kernel function that captures microstructural effects using material length scale parameters.

Beam theories were initially reformulated by considering the nonlocal differential constitutive relations of Eringen to solve the buckling load of beams with simply supported ends [20, 21]. A nonlocal strain gradient theory was developed and the geometric nonlinear effect due to the mid-plane stretching was also considered to perform buckling analysis of simply supported size-dependent beams [22]. The differential form of Eringen's model was subsequently found to be inadequate in addressing the size-dependent effect of columns, except for the column with hinged ends. Thus, the literature focused on the buckling analysis of minuscule columns using different kinds of analysis schemes, such as the integral form of Eringen's equation [23], discrete singular convolution method [24], and finite element formulation based on the minimum total potential energy principle [25, 26]. Three boundary conditions of columns containing hinged–hinged, clamped–hinged, and clamped–clamped ends were then used in the buckling analysis via a conformable fractional nonlocal model [27]. Published data concerning the influence of material length scale on the variation of critical buckling load in the case of distributed and combined load scenarios are limited. The buckling load of minuscule columns with a nonuniform moment of inertia, which is often encountered in real applications, should also be examined.

The governing equations of columns are formulated in the current research within the framework of Eringen's nonlocal elasticity. Due to the complexity induced by the nonlocal constitutive law in an integral form for any selected attenuation kernel, the analytical or closed-form solution of the key governing equation cannot be, if it is not impossible, readily obtained. Therefore, it is more appealing to adopt a numerical solution procedure to tackle such problem. In the present study, the finite element method is chosen due to its vast features, capability to handle general data, and simplicity in the formulation and numerical implementations. Columns with a uniform moment of inertia and those with a nonuniform cross-section are investigated herein to understand the effects of boundary conditions and material length scale on the buckling load of nanocolumns.

2. Theoretical Formulation

The eigenproblem governing the buckling state of the nonprismatic and nonlocal column (Fig. 1) can be formulated on the basis of the following basic equations:

$$\kappa(x) = w''(x) \tag{1}$$

$$\begin{aligned} M(x) &= \int_0^l K(x-\xi, l_0)\, EI(\xi)\, \kappa(\xi)\, d\xi \\ &\quad + \{1 - f(x)\}\, EI(x)\, \kappa(x) \end{aligned} \tag{2}$$

$$f(x) = \int_0^l K(x-\xi, l_0)\, d\xi$$

$$\begin{aligned} M'(x) + P(x) w'(x) &= V \\ V'(x) &= 0 \end{aligned} \tag{3}$$

$$P(x) = P + \int_x^l q(\xi)\, d\xi = P + \lambda \int_x^l q_0(\xi)\, d\xi \tag{4}$$

where E denotes Young's modulus; $I = I(x)$ denotes the moment of inertia of the cross-section; $K(x-\xi, l_0)$ is the selected attenuation function with l_0 representing the internal length scale of the material; $M(x)$ denotes the bending moment of the cross-section; P is the compression force applied at the top of the column; and $q(x) = \lambda q_0(x)$ is the distributed load represented by the load factor λ and the variation function $q_0(x)$. $V(x)$ and $w(x)$, respectively, denote the shearing force and the deflection of the cross-section.

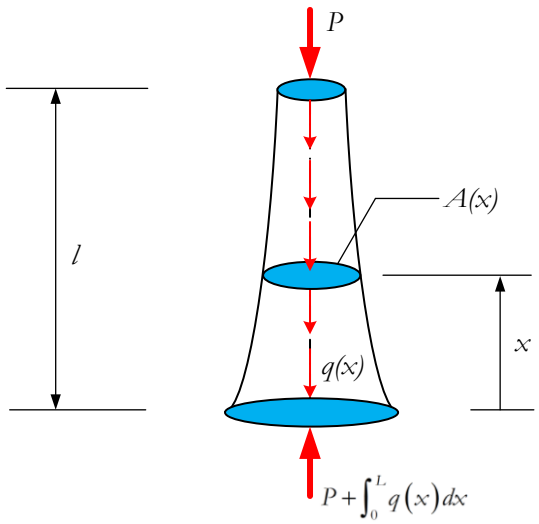

Fig. 1. Schematic of a perfectly straight column considered in this research.

The weak-form equation of Eq. (3), together with the kinematics given by Eq. (1) and the nonlocal moment–curvature relation given by Eq. (2), is given by

$$\begin{aligned}&\int_0^l v''(x)\int_0^l K(x-\xi,l_0)EI(\xi)w''(\xi)d\xi dx\\&+\int_0^1\{1-f(x)\}EI(x)v''(\bar{x})w''(x)dx\\&=\int_0^l P(x)v'(x)w'(x)dx\end{aligned}\tag{5}$$

where v is any sufficiently smooth test function. Substituting Eq. (4) into Eq. (5) yields:

$$\begin{aligned}&\int_0^l v''(x)\int_0^l K(x-\xi,l_0)EI(\xi)w''(\xi)d\xi dx\\&+\int_0^1\{1-f(x)\}EI(x)v''(\bar{x})w''(x)dx\\&=P\int_0^l v'(x)w'(x)dx\\&+\lambda\int_0^l p(x)v'(x)w'(x)dx\end{aligned}\tag{6}$$

where the function $p(x)$ is defined as

$$p(x)=\int_x^l q_0(\xi)d\xi\tag{7}$$

By introducing the following normalizations, including $\bar{x}=x/l$, $\bar{\xi}=\xi/l$, $\bar{l}=l/l_0$, $\bar{v}=v/l$, $\bar{w}=w/l$, $\bar{I}=I/I_0$, $\bar{K}(\bar{x}-\bar{\xi},\bar{l})=lK(x-\xi,l_0)$, $\bar{P}=Pl^2/EI_0$, $\bar{p}=pl^2/EI_0$, and $\bar{q}_0=q_0l/EI_0$, the weak-form equation (6) then becomes:

$$\begin{aligned}&\int_0^1\bar{v}''(\bar{x})\int_0^1\bar{K}(\bar{x}-\bar{\xi},\bar{l})\bar{I}(\bar{\xi})\bar{w}''(\bar{\xi})d\bar{\xi}d\bar{x}\\&+\int_0^1\{1-f(\bar{x})\}\bar{I}(\bar{x})\bar{v}''(\bar{x})\bar{w}''(\bar{x})d\bar{x}\\&=\bar{P}\int_0^1\bar{v}'(\bar{x})\bar{w}'(\bar{x})d\bar{x}\\&+\lambda\int_0^l\bar{p}(\bar{x})\bar{v}'(\bar{x})\bar{w}'(\bar{x})d\bar{x}\end{aligned}\tag{8}$$

where the function $f(\bar{x})$ is defined as

$$f(\bar{x})=\int_0^1\bar{K}(\bar{x}-\bar{\xi},\bar{l})d\bar{\xi}\tag{9}$$

Let the normalized interval $[0,1]$ be partitioned into n finite elements, that is, $[0,1]=\cup_{e=1,n}\Omega_e$, where $\Omega_e=[\bar{x}_{e-1},\bar{x}_e]$, $\bar{x}_0=0$, and $\bar{x}_n=1$, and the normalized deflection and test function over a generic element Ω_e can be approximated by:

$$\bar{w}^e(\bar{x}^e)=\boldsymbol{N}^e(\bar{x}^e)\boldsymbol{w}^e;\quad\bar{v}^e(\bar{x}^e)=\boldsymbol{N}^e(\bar{x}^e)\boldsymbol{u}^e\tag{10}$$

where $\bar{x}^e=\bar{x}-\bar{x}_{e-1}$; $\boldsymbol{w}^e=\{\bar{w}_1^e\quad\theta_1^e\quad\bar{w}_2^e\quad\theta_2^e\}^T$ is a vector containing the normalized end displacements $\bar{w}_1^e$, $\bar{w}_2^e$ and the end rotations θ_1^e, θ_2^e; $\boldsymbol{N}^e$ is a row matrix containing element shape function defined by

$$\boldsymbol{N}^e(\bar{x}^e)=\begin{bmatrix}1-3(\eta^e)^2+2(\eta^e)^3\\\bar{h}^e\eta^e(1-\eta^e)^2\\(\eta^e)^2(3-2\eta^e)\\\bar{h}^e(\eta^e)^2(\eta^e-1)\end{bmatrix}^T$$

where $\bar{h}^e=\bar{x}_e-\bar{x}_{e-1}$ and $\eta^e=\bar{x}^e/\bar{h}^e$; and $\boldsymbol{u}^e$ is an arbitrary vector. The normalized moment of inertia $\bar{A}(\bar{x})$ is represented by a piecewise constant function over the finite element mesh; in particular, the normalized moment of inertia of a generic element Ω_e is denoted by a constant $\bar{I}^e$. Based on the discretization (10) and the representation of the normalized moment of inertia by a piecewise constant function, the weak-form equation (8) then becomes:

$$(\boldsymbol{K}-\bar{P}\,\boldsymbol{M}_1-\lambda\,\boldsymbol{M}_2)\boldsymbol{U}=0\tag{11}$$

where $\boldsymbol{U}$ is a vector containing all degrees of freedom of the discretized column and the elastic stiffness matrix $\boldsymbol{K}$ and geometric stiffness matrix $\boldsymbol{M}$ are defined by

$$\boldsymbol{K} = \sum_{p=1}^{n}\sum_{q=1}^{n} \bar{l}^{\,q}\, \bar{\boldsymbol{k}}^{(p,q)} + \sum_{p=1}^{n} \bar{l}^{\,p}\, \hat{\boldsymbol{k}}^{(p)} \tag{12}$$

$$\boldsymbol{M_1} = \sum_{p=1}^{n} \boldsymbol{m_1^{(p)}} \tag{13}$$

$$\boldsymbol{M_2} = \sum_{p=1}^{n} \boldsymbol{m_2^{(p)}} \tag{14}$$

where $\bar{\boldsymbol{k}}^{(p,q)}$, $\hat{\boldsymbol{k}}^{(p)}$, $\boldsymbol{m_1^{(p)}}$ and $\boldsymbol{m_2^{(p)}}$ are respectively defined locally by:

$$\bar{\boldsymbol{k}}^{(p,q)} = \int_{\Omega_p} \left(\boldsymbol{C}^q\left(\bar{\xi}^{\,q}\right)\right)^T \int_{\Omega_q} \bar{K}\left(\bar{x}\left(\bar{x}^{\,p}\right) - \bar{\xi}\left(\bar{\xi}^{\,q}\right), \bar{l}\right) \boldsymbol{C}^q\left(\bar{\xi}^{\,q}\right) d\bar{\xi}^{\,q}\, d\bar{x}^{\,p} \tag{15}$$

$$\hat{\boldsymbol{k}}^{(p)} = \int_{\Omega_p} \left\{1 - f\left(\bar{x}\left(\bar{x}^{\,p}\right)\right)\right\} \left(\boldsymbol{C}^p\left(\bar{x}^{\,p}\right)\right)^T \boldsymbol{C}^p\left(\bar{x}^{\,p}\right) d\bar{x}^{\,p} \tag{16}$$

$$\boldsymbol{m_1^{(p)}} = \int_{\Omega_p} \left(\boldsymbol{B}^p\right)^T \boldsymbol{B}^p\, d\bar{x}^{\,p} \tag{17}$$

$$\boldsymbol{m_2^{(p)}} = \int_{\Omega_p} \bar{p}\left(\bar{x}\left(\bar{x}^{\,p}\right)\right) \left(\boldsymbol{B}^p\right)^T \boldsymbol{B}^p\, d\bar{x}^{\,p} \tag{18}$$

where $\bar{\xi}^{\,q} = \bar{\xi} - \bar{x}_{q-1}$, $\boldsymbol{B}^p = d\,\boldsymbol{N}^p / d\bar{x}^{\,p}$, and $\boldsymbol{C}^p = d\,\boldsymbol{B}^p / d\bar{x}^{\,p}$. Note that $\bar{\boldsymbol{k}}^{(p,q)}$ and $\hat{\boldsymbol{k}}^{(p)}$ can be viewed as the elastic stiffness matrices contributed from a pair of elements p, q and an element p, respectively, whereas $\boldsymbol{m_1^{(p)}}$ and $\boldsymbol{m_2^{(p)}}$ are the geometric stiffness matrixes contributed from an element p due to the presence of the concentrated and distributed loads, respectively. The function $\bar{p}$ ($\bar{x}$ ($\bar{x}^{\,p}$)) on the element Ω_p in Eq. (18) can be further approximated by linear interpolation functions as shown below to simplify the calculations of the matrix $\boldsymbol{m_2^{(p)}}$:

$$\bar{p}\left(\bar{x}\left(\bar{x}^{\,p}\right)\right) = \bar{p}_1^{\,p}\varphi_1^p\left(\bar{x}^{\,p}\right) + \bar{p}_2^{\,p}\varphi_2^p\left(\bar{x}^{\,p}\right) \tag{19}$$

where $\varphi_1^p\left(\bar{x}^{\,p}\right) = 1 - \eta^{\,p}$, $\varphi_2^p\left(\bar{x}^{\,p}\right) = \eta^{\,p}$, and $\bar{p}_1^{\,p}$, $\bar{p}_2^{\,p}$ are values of the function $\bar{p}$ ($\bar{x}$ ($\bar{x}^{\,p}$)) at the left and right end of the element Ω_p, respectively. By Substituting Eq. (19) into Eq. (18) results in:

$$\boldsymbol{m_2^{(p)}} = \bar{p}_1^{\,p}\, \boldsymbol{m_{21}^{(p)}} + \bar{p}_2^{\,p}\, \boldsymbol{m_{22}^{(p)}} \tag{20}$$

where the matrices $\boldsymbol{m_{21}^{(p)}}$ and $\boldsymbol{m_{22}^{(p)}}$ are defined as in Eqs. (21) and (22), respectively.

$$\boldsymbol{m_{21}^{(p)}} = \int_{\Omega_p} \varphi_1^p\left(\bar{x}^{\,p}\right) \left(\boldsymbol{B}^p\right)^T \boldsymbol{B}^p\, d\bar{x}^{\,p} \tag{21}$$

$$\boldsymbol{m_{22}^{(p)}} = \int_{\Omega_p} \varphi_2^p\left(\bar{x}^{\,p}\right) \left(\boldsymbol{B}^p\right)^T \boldsymbol{B}^p\, d\bar{x}^{\,p} \tag{22}$$

Notably, all the matrices $\bar{\boldsymbol{k}}^{(p,q)}$, $\hat{\boldsymbol{k}}^{(p)}$, $\boldsymbol{m_1^{(p)}}$, $\boldsymbol{m_{21}^{(p)}}$, and $\boldsymbol{m_{22}^{(p)}}$ can be derived in a closed form.

3. Numerical Results and Discussions

The obtained results from the current computational work are initially compared with those of classical column theory to verify the formulation. Three types of end conditions, such as clamped end (C), hinged end (H), and free end (F), have been investigated in the research:

$$\text{Clamped end:} \quad w = 0, \quad \frac{dw}{dx} = 0$$

$$\text{Hinged end:} \quad w = 0, \quad M = 0$$

$$\text{Free end:} \quad V = 0, \quad M = 0$$

The load cases observed in the current work are listed as follows:

$$\text{Uniform } (m = 0): \quad \bar{q}_0 = \left(1 - \bar{x}\right)^0 = 1$$

$$\text{Linear } (m = 1): \quad \bar{q}_0 = \left(1 - \bar{x}\right)^1$$

$$\text{Quadratic } (m = 2): \quad \bar{q}_0 = \left(1 - \bar{x}\right)^2$$

where m is the exponent number controlling axial load distribution in columns. In the numerical study, the following attenuation function $K\left(x - \xi, l_0\right) = e^{-|x-\xi|/l_0} / 2l_0$ is considered.

The numerical results presented in Tables 1–4 aim to determine the convergence behavior for solutions of columns with a uniform moment of inertia subjected to various loading scenarios throughout this research. Herein, a convergence indicator is defined as the calculated buckling load from each normalized mesh considering those obtained from the case using 128 elements. It is seen that the convergence behavior of numerical solutions depends on the boundary conditions, normalized length parameter $\bar{l}$, and applied loads. In particular, buckling solutions of the C-F column converge faster than that of the other three boundary conditions for all load cases considered and finer meshes are generally required as the length scale parameter $\bar{l}$ decreases and load cases with the presence of distributed axial force. The mesh containing 32 elements then meets the minimum

requirement of convergence validity with a relative error of less than 1%.

A component with a nonuniform cross-sectional area and moment of inertia (Fig. 2) has found broad application in optomechanical sensing and laser beam scanning systems [6, 28]. Note that nano-elements with variable cross sections serve either to tune a system to a specific frequency spectrum or enhance its mechanical sensitivity to external excitations. Predicting physical responses of nano-beams such as buckling phenomena, taking their geometry and nano-scale influences into account, is an essential issue in the design of nano-mechanical systems.

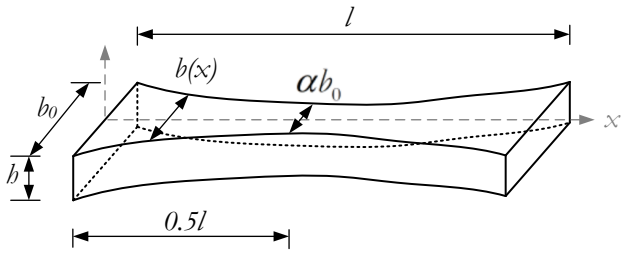

Fig. 2. Schematic of a perfectly straight column with the parabolically varying cross-sectional area.

The cross-section is rectangular with constant thickness h, and the height varies as a function such that:

$$b(\bar{x}) = b_0\left\{1+4(1-\alpha)\left(\bar{x}^2-\bar{x}\right)\right\} \tag{23}$$

where α denotes the dimensionless parameter for classifying the degree of convexity (or concavity) of the parabolic curve, and b_0 represents the maximum width at end columns. The height function (23) can be rewritten considering normalized moment of inertia as follows:

$$\bar{I}(\bar{x}) = \left\{1+4(1-\alpha)\left(\bar{x}^2-\bar{x}\right)\right\}^3 \tag{24}$$

The convergence of computed buckling loads for a parabolic column is also investigated for C-F, H-H, C-H, and C-C end conditions, $\bar{l} \in \{1,10\}$, and various load cases, and results are reported in Tables 5–8. A similar conclusion on the convergence behavior of numerical solutions to the case of the uniform column can be drawn except that finer meshes are generally required for this particular column to achieve the same level of accuracy.

3.1. Column Subjected to Concentrated Loading

The normalized buckling concentrated load, which is the buckling concentrated load at a considered material length scale (P_{cr}^0) divided by the classical eigenvalue buckling concentrated load (P_{cr}^{0c}) [29], is defined to assess the variation of the buckling resistance capacity of columns while focusing on the size effect and the positive dimensionless parameter controlling the parabolic curve shape of columns. As observed in Fig. 3, a buckling load converges to the classical eigenvalue buckling load for substantially small (i.e., $\bar{l} < 0.1$) and large (i.e., $\bar{l} > 50$) values of material length scale. The buckling load for all four boundary conditions is dramatically decreased at the normalized material length scale between 1 and 10. The C–C column provides the strongest influence of decreasing a buckling concentrated load of columns, while the least effect is revealed in those with C–F end conditions. The increase in the dimensionless parameter controlling the shape of the parabolic curve will raise the normalized concentrated buckling load of columns, except for the C–F end condition, in which the effect of column shape on buckling load is insignificantly changed. When $\alpha = 2$, size-dependent behavior has the lowest impact on normalized buckling concentrated load in most boundary conditions, particularly in the case of H–H columns. However, different from the C–F column, uniform columns ($\alpha = 1$) exhibit the slightest influence of size-dependent buckling concentrated load on normalized buckling compared to those with nonuniform columns.

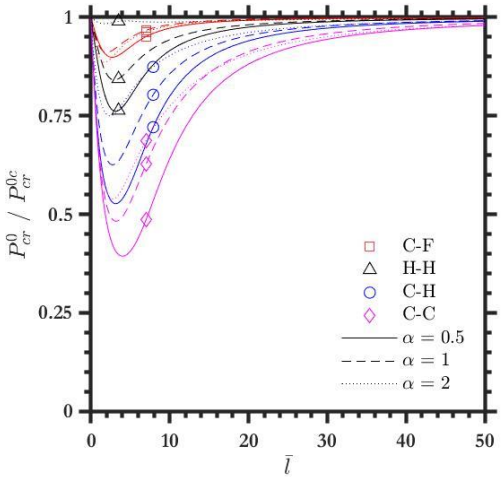

Fig. 3. Normalized buckling concentrated load versus normalized material external length scale of columns subjected to concentrated loading.

3.2. Column Subjected to Distributed Loading Along its Length

The normalized buckling distributed load is defined by the ratio between the buckling distributed load at a considered material length scale (λ_{cr}^0) and the classical eigenvalue buckling distributed load (λ_{cr}^{0c}) to observe the buckling load capacity of columns subjected to distributed loading [29]. A nearly similar behavior, with a column subjected to concentrated loading, is also found in Fig. 4. Columns subjected to the distributed loads (i.e., uniformly distributed, linearly distributed, and parabolic distributed loads) demonstrate a quite similar trend for the decrease

DOI:10.4186/ej.2022.26.10.73

in buckling distributed load at the normalized material length scale between 1 and 10. The uniformly distributed load ($m=0$) and the parabolic distribution ($m=2$) of the axially applied force are respectively the most and the least buckling distributed load except for the H–H end condition, which is the opposite of findings in three previous end conditions.

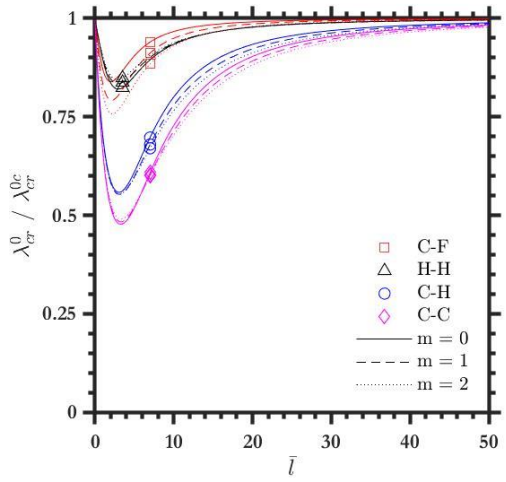

Fig. 4. Normalized buckling distributed load versus normalized material external length scale of uniform columns subjected to various distributed loadings.

The effect of the positive dimensionless parameters controlling the shape of the parabolic curve on normalized distributed buckling loads is also investigated in Fig. 5. For all considered distributed loading configurations, the C–F and H–H columns respectively demonstrate the least prominent size-dependent effect on normalized distributed buckling load at $\alpha=0.5$ and $\alpha=2$. The size-dependent effect has a negligible influence on the normalized distributed buckling loads of C–H and C–C columns with $\alpha=2$ compared to those with $\alpha=0.5$ and the case of uniform columns, while the normalized material length scales are less than eight. However, the results are paradoxical when the normalized material length scales exceed eight. The uniform columns are then the case wherein size-dependent buckling load has a negligible effect on normalized distributed buckling load.

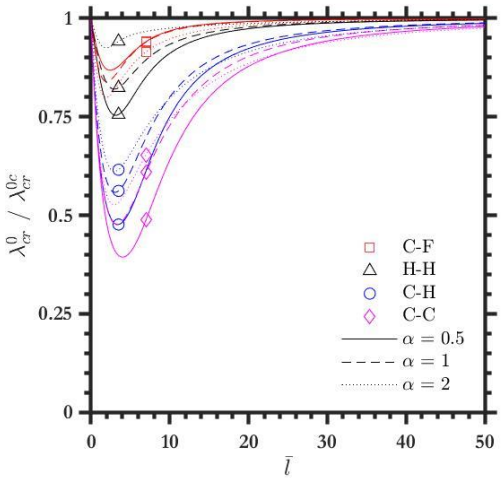

(a) Uniformly distributed load

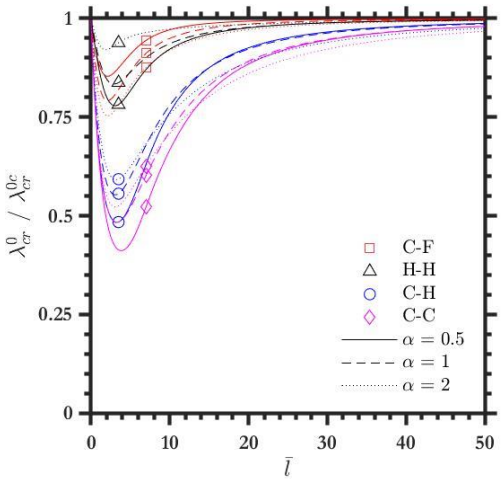

(b) Linearly distributed load

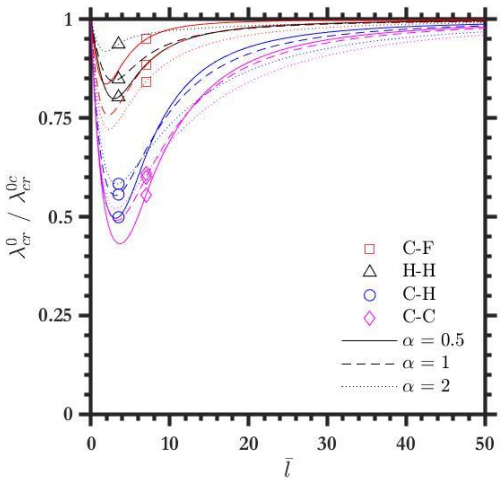

(c) Parabolic distributed load

Fig. 5. Effect of dimensionless parameter controlling the shape of the parabolic curve on normalized buckling distributed load of columns subjected to various distributed loadings.

Table 1. Normalized buckling load of uniform columns subjected to concentrated loading for convergence study.

n	$P^{(n)} / P^{(128)}$							
	C–F column		**H–H column**		**C–H column**		**C–C column**	
	$\overline{l}=1$	$\overline{l}=10$	$\overline{l}=1$	$\overline{l}=10$	$\overline{l}=1$	$\overline{l}=10$	$\overline{l}=1$	$\overline{l}=10$
2	1.000786	1.000474	1.006573	1.005558	1.024692	1.012779	1.015662	1.020261
4	1.000052	1.000015	1.000666	1.000109	1.002332	1.000683	1.008186	1.003032
8	1.000004	1.000001	1.000045	1.000013	1.000155	1.000041	1.000544	1.000111
16	1.000001	1.000000	1.000003	1.000001	1.000010	1.000002	1.000035	1.000006
32	1.000001	1.000000	1.000001	1.000000	1.000001	1.000000	1.000002	1.000000
64	1.000001	1.000000	1.000000	1.000000	1.000000	1.000000	1.000000	1.000000
128	1.000000	1.000000	1.000000	1.000000	1.000000	1.000000	1.000000	1.000000

Table 2. Normalized buckling load of uniform columns subjected to uniformly distributed loading for convergence study.

n	$\lambda^{(n)} / \lambda^{(128)}$							
	C–F column		**H–H column**		**C–H column**		**C–C column**	
	$\overline{l}=1$	$\overline{l}=10$	$\overline{l}=1$	$\overline{l}=10$	$\overline{l}=1$	$\overline{l}=10$	$\overline{l}=1$	$\overline{l}=10$
2	1.004234	1.001779	1.026398	1.016893	1.012962	1.014164	1.041234	1.026724
4	1.000319	1.000132	1.001334	1.000231	1.006943	1.004085	1.011862	1.007208
8	1.000021	1.000005	1.000089	1.000025	1.000481	1.000158	1.000855	1.000277
16	1.000002	1.000000	1.000006	1.000002	1.000031	1.000009	1.000055	1.000017
32	1.000001	1.000000	1.000001	1.000000	1.000002	1.000001	1.000004	1.000001
64	1.000001	1.000000	1.000000	1.000000	1.000000	1.000000	1.000000	1.000000
128	1.000000	1.000000	1.000000	1.000000	1.000000	1.000000	1.000000	1.000000

Table 3. Normalized buckling load of uniform columns subjected to linearly distributed loading for convergence study.

n	$\lambda^{(n)} / \lambda^{(128)}$							
	C–F column		**H–H column**		**C–H column**		**C–C column**	
	$\overline{l}=1$	$\overline{l}=10$	$\overline{l}=1$	$\overline{l}=10$	$\overline{l}=1$	$\overline{l}=10$	$\overline{l}=1$	$\overline{l}=10$
2	0.828233	0.815990	0.953317	0.944753	0.885912	0.892710	0.940061	0.939415
4	0.951953	0.948037	0.980602	0.978759	0.976572	0.978831	0.986873	0.989497
8	0.987551	0.986539	0.994754	0.994582	0.992795	0.993083	0.995029	0.994945
16	0.996893	0.996643	0.998677	0.998652	0.998071	0.998208	0.998529	0.998621
32	0.999259	0.999199	0.999684	0.999678	0.999531	0.999569	0.999634	0.999664
64	0.999852	0.999840	0.999937	0.999936	0.999906	0.999913	0.999926	0.999932
128	1.000000	1.000000	1.000000	1.000000	1.000000	1.000000	1.000000	1.000000

Table 4. Normalized buckling load of uniform columns subjected to 50% of the classical eigenvalue concentrated buckling load together with uniformly distributed loading for convergence study.

n	$\lambda^{(n)} / \lambda^{(128)}$							
	C–F column		**H–H column**		**C–H column**		**C–C column**	
	$\overline{l}=1$	$\overline{l}=10$	$\overline{l}=1$	$\overline{l}=10$	$\overline{l}=1$	$\overline{l}=10$	$\overline{l}=1$	$\overline{l}=10$
2	1.004095	1.001417	1.024679	1.017581	1.040015	1.018394	1.071559	1.060748
4	1.000274	1.000106	1.001786	1.000290	1.009935	1.003884	1.034669	1.010740
8	1.000020	1.000005	1.000120	1.000034	1.000664	1.000162	1.002311	1.000391
16	1.000004	1.000000	1.000008	1.000002	1.000043	1.000009	1.000148	1.000022
32	1.000003	1.000000	1.000001	1.000000	1.000003	1.000001	1.000010	1.000001
64	1.000003	1.000000	1.000001	1.000000	1.000001	1.000000	1.000001	1.000000
128	1.000000	1.000000	1.000000	1.000000	1.000000	1.000000	1.000000	1.000000

Table 5. Normalized buckling load of parabolic columns with $\alpha = 2$ subjected to concentrated loading for convergence study.

n	$P^{(n)} / P^{(128)}$							
	C–F column		**H–H column**		**C–H column**		**C–C column**	
	$\overline{l} = 1$	$\overline{l} = 10$	$\overline{l} = 1$	$\overline{l} = 10$	$\overline{l} = 1$	$\overline{l} = 10$	$\overline{l} = 1$	$\overline{l} = 10$
2	1.325382	1.290219	0.687875	0.710026	0.919501	0.950991	1.167209	1.153105
4	1.240282	1.221980	0.879768	0.883226	0.993672	1.008412	1.233898	1.233554
8	1.088680	1.083160	0.966528	0.968035	1.005443	1.012444	1.079631	1.071137
16	1.025250	1.023823	0.992055	0.992272	1.002786	1.004659	1.021696	1.019305
32	1.006277	1.005932	0.998164	0.998193	1.000793	1.001243	1.005303	1.004739
64	1.001271	1.001201	0.999636	0.999641	1.000166	1.000256	1.001068	1.000956
128	1.000000	1.000000	1.000000	1.000000	1.000000	1.000000	1.000000	1.000000

Table 6. Normalized buckling load of parabolic columns with $\alpha = 2$ subjected to uniformly distributed loading for convergence study.

n	$\lambda^{(n)} / \lambda^{(128)}$							
	C–F column		**H–H column**		**C–H column**		**C–C column**	
	$\overline{l} = 1$	$\overline{l} = 10$	$\overline{l} = 1$	$\overline{l} = 10$	$\overline{l} = 1$	$\overline{l} = 10$	$\overline{l} = 1$	$\overline{l} = 10$
2	1.642382	1.601371	0.762583	0.760758	1.002284	1.063712	1.237752	1.219612
4	1.362146	1.345820	0.894627	0.880497	1.144030	1.193958	1.259746	1.283034
8	1.121812	1.117155	0.967127	0.966300	1.057225	1.060017	1.091175	1.083769
16	1.033621	1.032506	0.992150	0.992177	1.015734	1.015727	1.024252	1.021411
32	1.008280	1.008020	0.998204	0.998203	1.003829	1.003826	1.005866	1.005185
64	1.001672	1.001619	0.999646	0.999644	1.000770	1.000770	1.001178	1.001042
128	1.000000	1.000000	1.000000	1.000000	1.000000	1.000000	1.000000	1.000000

Table 7. Normalized buckling load of parabolic columns with $\alpha = 2$ subjected to linearly distributed loading for convergence study.

n	$\lambda^{(n)} / \lambda^{(128)}$							
	C–F column		**H–H column**		**C–H column**		**C–C column**	
	$\overline{l} = 1$	$\overline{l} = 10$	$\overline{l} = 1$	$\overline{l} = 10$	$\overline{l} = 1$	$\overline{l} = 10$	$\overline{l} = 1$	$\overline{l} = 10$
2	1.559517	1.523849	0.759419	0.753360	0.989054	1.075045	1.231706	1.258016
4	1.398483	1.385319	0.890533	0.865431	1.188304	1.249844	1.290879	1.310091
8	1.136392	1.131837	0.962937	0.959729	1.080633	1.085207	1.114011	1.110410
16	1.037593	1.036498	0.991047	0.990891	1.021659	1.021022	1.029852	1.026499
32	1.009246	1.008993	0.997965	0.997937	1.005200	1.005030	1.007138	1.006314
64	1.001866	1.001815	0.999600	0.999594	1.001041	1.001008	1.001428	1.001264
128	1.000000	1.000000	1.000000	1.000000	1.000000	1.000000	1.000000	1.000000

Table 8. Normalized buckling load of parabolic columns with $\alpha = 2$ subjected to 50% of the classical eigenvalue concentrated buckling load together with uniformly distributed loading for convergence study.

n	$\lambda^{(n)} / \lambda^{(128)}$							
	C–F column		**H–H column**		**C–H column**		**C–C column**	
	$\overline{l} = 1$	$\overline{l} = 10$	$\overline{l} = 1$	$\overline{l} = 10$	$\overline{l} = 1$	$\overline{l} = 10$	$\overline{l} = 1$	$\overline{l} = 10$
2	1.720671	1.664022	0.728798	0.730966	0.977509	1.048686	1.267372	1.241028
4	1.412261	1.387819	0.883951	0.871003	1.143249	1.197197	1.310373	1.324836
8	1.139064	1.131831	0.964388	0.963777	1.058381	1.062121	1.107645	1.095595
16	1.038417	1.036610	0.991504	0.991548	1.016246	1.016466	1.028772	1.024739
32	1.009465	1.009035	0.998054	0.998054	1.003970	1.004018	1.006977	1.006009
64	1.001912	1.001824	0.999616	0.999615	1.000799	1.000809	1.001402	1.001208
128	1.000000	1.000000	1.000000	1.000000	1.000000	1.000000	1.000000	1.000000

3.3. Column Under Combined Concentrated and Uniformly Distributed Loads

The diagrams showing the interaction between normalized buckling concentrated and normalized uniform distributed loads are demonstrated in Fig. 6. This interaction is evident from Eq. (11) because the buckling concentrated load always has a simple linear relationship with the buckling distributed load. This finding also indicates that the interaction curves are unaffected by boundary conditions, column shapes, and material length scale parameters.

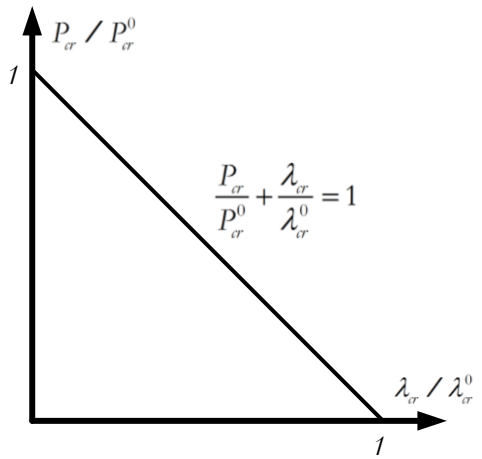

Fig. 6. Interaction diagrams of columns subjected to combined concentrated and uniformly distributed loads.

4. Conclusions

This research employs a direct technique based on the conventional finite element discretization and the size-dependent behavior via nonlocal elasticity to capture the effects of boundary conditions and material length scale parameters on the buckling load of columns. The approximate buckling load obtained using finite element analysis is compared with the exact solution based on the classical eigenvalue buckling load. The following conclusions are drawn.

- The buckling load is significantly reduced for concentrated and distributed load scenarios when the normalized material length scale is between 1 and 10.
- A buckling concentrated load of columns is reduced proportionally to the increase in an applied buckling uniform distributed load for all end conditions and the normalized material length scales. The effect is similar to that of columns subjected to a prescribed concentrated load, which is less than the classical eigenvalue concentrated buckling load.
- An increase in the concavity (or convexity) of parabolic columns will impact the concentrated and uniformly distributed buckling loads.

Acknowledgment

This research work was financially supported by the Office of the Permanent Secretary, MHESI (Ministry of Higher Education, Science, Research, and Innovation) with grant No. RGNS 64-0103. The first author is also grateful to the support provided by the Faculty of Engineering and Architecture, Rajamangala University of Technology Tawan-ok, Bangkok, Thailand.

References

[1] G.-Y. Su, Y.-X. Li, X.-Y. Li, and R. Müller, "Free and forced vibrations of nanowires on elastic substrates," *International Journal of Mechanical Sciences*, vol. 138-139, pp. 62-73, 2018, doi: https://doi.org/10.1016/j.ijmecsci.2018.01.039.

[2] W. Xiao, F. Wang, and J. Liu, "Analysis of axial compressive loaded beam under random support excitations," *Journal of Sound and Vibration*, vol. 410, pp. 378-388, 2017, doi: https://doi.org/10.1016/j.jsv.2017.08.045.

[3] C. C. Huang, S. C. Peng, W. Y. Lin, F. Fujii, and K. M. Hsiao, "A buckling and postbuckling analysis of axially loaded thin-walled beams with point-symmetric open section using corotational finite element formulation," *Thin-Walled Structures*, vol. 124, pp. 558-573, 2018, doi: https://doi.org/10.1016/j.tws.2017.11.056.

[4] Y. M. Lin, C. Dimitrakopoulos, K. A. Jenkins, D. B. Farmer, H. Y. Chiu, A. Grill, and Ph. Avouris, "100-GHz transistors from wafer-scale epitaxial graphene," *Science*, vol. 327, no. 5966, p. 662, 2010, doi: https://10.1126/science.1184289.

[5] H. Pfeifer, T. Paraïso, L. Zang, and O. Painter, "Design of tunable GHz-frequency optomechanical crystal resonators," *Optics Express*, vol. 24, 2016, doi: https://10.1364/OE.24.011407.

[6] B. H. Ahn, J. H. Kang, M. K. Kim, J. H. Song, B. Min, K. S. Kim, and Y. H. Lee, "One-dimensional parabolic-beam photonic crystal laser," *Optics Express*, vol. 18, pp. 5654-5660, 2010, doi: https://10.1364/OE.18.005654.

[7] K. Y. Jeong, Y. S. No, Y. Hwang, K. S. Kim, M. K. Seo, H. G. Park and Y. H. Lee, "Electrically driven nanobeam laser," *Nature Communications*, vol. 4, no. 1, p. 2822, 2013, doi: https://10.1038/ncomms3822.

[8] T. Juarez, A. Schroer, R. Schwaiger, and A. M. Hodge, "Evaluating sputter deposited metal coatings on 3D printed polymer micro-truss structures," *Materials and Design*, vol. 140, pp. 442-450, 2018, doi: https://doi.org/10.1016/j.matdes.2017.12.005.

[9] Y. Y. Zhang, C. M. Wang, W. H. Duan, Y. Xiang, and Z. Zong, "Assessment of continuum mechanics models in predicting buckling strains of single-walled carbon nanotubes," *Nanotechnology*, vol. 20, no. 39, p. 395707, 2009, doi: https://10.1088/0957-4484/20/39/395707.

[10] Y. S. Li and T. Xiao, "Free vibration of the one-dimensional piezoelectric quasicrystal microbeams based on modified couple stress theory," *Applied Mathematical Modelling*, vol. 96, pp. 733-750, 2021, doi: https://doi.org/10.1016/j.apm.2021.03.028.

[11] B. Akgöz and Ö. Civalek, "Vibrational characteristics of embedded microbeams lying on a two-parameter elastic foundation in thermal environment," *Composites Part B: Engineering*, vol. 150, pp. 68-77, 2018, doi: https://doi.org/10.1016/j.compositesb.2018.05.049.

[12] R. A. Shanab and M. A. Attia, "Semi-analytical solutions for static and dynamic responses of bi-directional functionally graded nonuniform nanobeams with surface energy effect," *Engineering with Computers*, 2020, doi: https://10.1007/s00366-020-01205-6.

[13] P. T. Thang, P. Tran, and T. Nguyen-Thoi, "Applying nonlocal strain gradient theory to size-dependent analysis of functionally graded carbon nanotube-reinforced composite nanoplates," *Applied Mathematical Modelling*, vol. 93, pp. 775-791, 2021, doi: https://doi.org/10.1016/j.apm.2021.01.001.

[14] A. A. Daikh, M. S. A. Houari, and M. A. Eltaher, "A novel nonlocal strain gradient Quasi-3D bending analysis of sigmoid functionally graded sandwich nanoplates," *Composite Structures*, vol. 262, p. 113347, 2021, doi: https://doi.org/10.1016/j.compstruct.2020.113347.

[15] P.-L. Bian, H. Qing, and C.-F. Gao, "One-dimensional stress-driven nonlocal integral model with bi-Helmholtz kernel: Close form solution and consistent size effect," *Applied Mathematical Modelling*, vol. 89, pp. 400-412, 2021, doi: https://doi.org/10.1016/j.apm.2020.07.058.

[16] R. Penna, L. Feo, A. Fortunato, and R. Luciano, "Nonlinear free vibrations analysis of geometrically imperfect FG nano-beams based on stress-driven nonlocal elasticity with initial pretension force," *Composite Structures*, vol. 255, p. 112856, 2021, doi: https://doi.org/10.1016/j.compstruct.2020.112856.

[17] U. Gul and M. Aydogdu, "Buckling analysis of functionally graded beams with periodic nanostructures using doublet mechanics theory," *Journal of the Brazilian Society of Mechanical Sciences and Engineering*, vol. 43, no. 5, p. 254, 2021, doi: https://10.1007/s40430-021-02972-z.

[18] M. A. Eltaher and N. Mohamed, "Nonlinear stability and vibration of imperfect CNTs by Doublet mechanics," *Applied Mathematics and Computation*, vol. 382, p. 125311, 2020, doi: https://doi.org/10.1016/j.amc.2020.125311.

[19] A. C. Eringen, "On differential equations of nonlocal elasticity and solutions of screw dislocation and surface waves," *Journal of Applied Physics*, vol. 54, pp. 4703-4710, 1983, doi: https://doi.org/10.1063/1.332803.

[20] J. N. Reddy, "Nonlocal theories for bending, buckling and vibration of beams," *International Journal of Engineering Science*, vol. 45, no. 2-8, pp. 288-307, 2007, doi: https://doi.org/10.1016/j.ijengsci.2007.04.004.

[21] H. T. Thai, "A nonlocal beam theory for bending, buckling, and vibration of nanobeams," *International Journal of Engineering Science*, vol. 52, pp. 56-64, 2012, doi: https://doi.org/10.1016/j.ijengsci.2011.11.011.

[22] L. Li and Y. Hu, "Buckling analysis of size-dependent nonlinear beams based on a nonlocal strain gradient theory," *International Journal of Engineering Science*, vol. 97, pp. 84-94, 2015, doi: https://doi.org/10.1016/j.ijengsci.2015.08.013.

[23] M. Tuna and M. Kirca, "Exact solution of Eringen's nonlocal integral model for vibration and buckling of Euler–Bernoulli beam," *International Journal of Engineering Science*, vol. 107, pp. 54-67, 2016, doi: https://doi.org/10.1016/j.ijengsci.2016.07.004.

[24] Ö. Civalek and O. Kiracioglu, "Free vibration analysis of Timoshenko beams by DSC method," *International Journal for Numerical Methods in Biomedical Engineering*, vol. 26, pp. 1890-1898, 2010, doi: https://doi.org/10.1002/cnm.1279.

[25] M. Tuna and M. Kirca, "Bending, buckling and free vibration analysis of Euler-Bernoulli nanobeams using Eringen's nonlocal integral model via finite element method," *Composite Structures*, vol. 179, pp. 269-284, 2017, doi: https://doi.org/10.1016/j.compstruct.2017.07.019.

[26] Ç. Demir, K. Mercan, H. M. Numanoglu, and Ö. Civalek, "Bending response of nanobeams resting on elastic foundation," *Journal of Applied and Computational Mechanics*, vol. 4, pp. 105-114, 2018, doi: https://dx.doi.org/10.22055/jacm.2017.22594.1137.

[27] S. K. Jena, S. Chakraverty, R. M. Jena, and F. Tornabene, "A novel fractional nonlocal model and its application in buckling analysis of Euler-Bernoulli nanobeam," *Materials Research Express*, vol. 6, no. 5, p. 055016, 2019, doi: http://dx.doi.org/10.1088/2053-1591/ab016b.

[28] G. Mikhasev, "Free high-frequency vibrations of nonlocally elastic beam with varying cross-section area," *Continuum Mechanics and Thermodynamics*, vol. 33, pp. 1299-1312, 2021, doi: https://doi.org/10.1007/s00161-021-00977-6.

[29] C. H. Yoo and S. C. Lee, "Special topics in elastic stability of columns," in *Stability of Structures*. Oxford, United Kingdom, 2011, ch. 2, pp. 75-153.

Tosporn Prasertsri, photograph and biography not available at the time of publication.

Suppawit Intratanoo, photograph and biography not available at the time of publication.

Thunyamas Jirajaran, photograph and biography not available at the time of publication.

Weeraporn Phongtinnaboot, photograph and biography not available at the time of publication.

Jaroon Rungamornrat, photograph and biography not available at the time of publication.